DE GRUYTER OPEN

Archives of Hydro-Engineering and Environmental Mechanics
Vol. 64 (2017), No. 2, pp. 115–137
DOI: 10.1515/heem-2017-0008

SPH Modelling of Sea-ice Pack Dynamics

Ryszard Staroszczyk

Institute of Hydro-Engineering, Polish Academy of Sciences, Kościerska 7, 80-328 Gdańsk, Poland

(Received November 19, 2017; revised December 27, 2017)

Abstract

The paper is concerned with the problem of sea-ice pack motion and deformation under the action of wind and water currents. Differential equations describing the dynamics of ice, with its very distinct material responses in converging and diverging flows, express the mass and linear momentum balances on the horizontal plane (the free surface of the ocean). These equations are solved by the fully Lagrangian method of smoothed particle hydrodynamics (SPH). Assuming that the ice behaviour can be approximated by a non-linearly viscous rheology, the proposed SPH model has been used to simulate the evolution of a sea-ice pack driven by wind drag stresses. The results of numerical simulations illustrate the evolution of an ice pack, including variations in ice thickness and ice area fraction in space and time. The effects of different initial ice pack configurations and of different conditions assumed at the coast–ice interface are examined. In particular, the SPH model is applied to a pack flow driven by a vortex wind to demonstrate how well the Lagrangian formulation can capture large deformations and displacements of sea ice.

Key words: sea-ice dynamics, Lagrangian description, smoothed particle hydrodynamics, moving boundary problem

List of Symbols

a	–	reference particle label;
A, A_0	–	ice concentration (ice area fraction);
A_f	–	critical ice concentration;
b	–	neighbouring particle label;
$C_a,\ C_w$	–	dimensionless wind and water drag coefficients;
d	–	initial inter-particle spacing;
$\boldsymbol{D}$	–	strain-rate tensor;
$f(A)$	–	ice–ice contact length function;
h, h_0	–	ice thickness;
$H(\cdot)$	–	Heaviside unit step function;
$\boldsymbol{I}$	–	unit tensor;
$\boldsymbol{k}$	–	upward vertical unit vector;
K	–	ice strength-compactness parameter;

m – mass;
$\boldsymbol{N}$ – depth-integrated horizontal stress tensor;
p – pressure;
R – smoothing kernel support radius;
t – time;
$\boldsymbol{u}_a$, $\boldsymbol{u}_w$ – wind and water current velocity vectors;
$\boldsymbol{v}$ – ice velocity vector;
W – SPH smoothing kernel function;
x_i $(i = 1, 2)$ – spatial Cartesian co-ordinates;
$\boldsymbol{x}$ – position vector;
$\alpha(A)$ – ice ridging function;
γ – shear-rate invariant;
ζ – ice bulk viscosity;
η – ice horizontal dilatation-rate;
μ – ice shear viscosity;
ρ – ice density;
ρ_{air}, ρ_w – air and water densities;
$\boldsymbol{\sigma}$ – Cauchy stress tensor;
$\boldsymbol{\tau}_a$, $\boldsymbol{\tau}_w$ – wind stress and water drag surface tractions;
ϕ_1, ϕ_2 – material viscous response functions;
Ω – Earth rotation angular velocity.

1. Introduction

A typical large-scale sea-ice pack is a complex thermodynamic system, consisting of a multitude of interacting floes of different size and geometry, driven by wind drag and ocean currents, and subject to surface and basal freezing and melting. As individual floes move about and collide, they break, merge and pile up on one another, giving rise to large variations in local ice thickness and ice concentration. Because of the very distinct behaviour of sea ice in converging and diverging flow regimes, interfaces separating converging and diverging regions in ice develop and subsequently propagate throughout the pack, often leading to the fragmentation of an initially coherent ice pack domain. An important feature is also a significant change in the geometry of a domain occupied by the pack, associated with the evolution of boundaries between the coherent ice and the open sea.

The majority of theoretical models describing the behaviour of sea ice, starting from the model developed by Hibler (1979), are based on the assumption that the ice cover can be treated as a two-dimensional continuum moving and deforming on the ocean surface. Hence, the equations governing the dynamic behaviour of sea ice are derived by the methodology of continuum mechanics. Conventional numerical models for solving ensuing differential equations, such as finite-difference

or finite-element methods, use computational grids/meshes on which discrete variables are defined. Since the sea ice equations are usually formulated in the spatial (Eulerian) coordinates, the application of the classical mesh-based methods involves numerical difficulties and high computational costs in all cases in which extensive displacements and deformations of ice occur. It is much more natural to formulate and solve the sea ice dynamics equations in the material (Lagrangian) coordinates, in which the movement of individual material points, and the mechanical behaviour of the medium at these points, can be easily traced in time. Compared to the Eulerian description, the Lagrangian method also has the advantage of increased numerical stability due to the absence of convective terms in the momentum equations set in the Eulerian framework. Additionally, the treatment of boundary conditions is formally more straightforward in the Lagrangian description, since these are imposed on material surfaces; that is, on surfaces which do not move in the referential coordinates.

One of the fully Lagrangian methods which seems to be well suited to solving sea ice dynamics problems, especially because of its mesh-free character which enables an effective treatment of propagating discontinuity fronts, is the Smoothed Particle Hydrodynamics (SPH) method. This method has been developed extensively in the past two decades and has been successfully employed in many branches of physics and engineering – examples can be found in two review papers by Monaghan (2005, 2012). The SPH method was also used to model the dynamics of floating ice, though rather rarely compared to other branches of applied mechanics. The first applications of the SPH approach to the sea-ice modelling were due to Gutfraind and Savage (1997, 1998), who simulated the behaviour of ice in the open sea; that is, in the absence of solid boundaries (coasts), which significantly simplifies numerical calculations. Another example was the work by Shen et al (2000), in which the SPH approach was employed to simulate the flow of river ice, with a focus on its jamming, in which case the movement of ice is severely restricted by solid boundaries (river banks). In the present work, an in-between case is investigated, in which there are some boundaries along which a sea-ice pack interacts with a coast, but there are also extensive boundaries along which ice interacts with the open sea. Such a case seems to be the most typical situation actually occurring in realistic sea-ice pack flows in near-coast waters, and is also regarded as the most challenging case from the viewpoint of numerical modelling (Schulkes et al 1998, Morland and Staroszczyk 1998).

An important aspect of sea ice modelling is the rheology of ice. Commonly, after Hibler (1977, 1979), sea ice is assumed to be a viscous-plastic material. As in any problem involving plastic flow, a special numerical treatment of the discretized equations is then required, which increases the complexity of the solution algorithm. For this reason, attempts have been made to use a simpler, viscous fluid rheology, which does not need a yield curve as part of the problem description. An example is the model proposed by Morland and Staroszczyk (1998) in which a non-linearly viscous fluid flow law is applied, in which maximum stresses are bounded in a way similar to the theory of plasticity. Here, a simpler version of the non-linearly viscous rheolog-

ical model is employed, stemming from the Reiner-Rivlin viscous fluid constitutive theory.

The SPH model developed in this work is used to simulate the dynamic behaviour of a large sea-ice field under the action of wind and ocean drag stresses. The results of the simulations illustrate the evolution of the ice pack, including variations in ice thickness and ice area fraction (ice concentration) in space and time. The effects of different initial ice pack configurations and of different conditions adopted at coast–ice boundaries are explored, with an interest in tracking changes in the position of boundaries between the open sea and the ice pack. In particular, the behaviour of the ice pack subject to the action of a vortex wind field is simulated, in order to show how well the proposed model can capture large deformations and displacements of the sea-ice pack and large displacements of its moving boundaries.

The paper is organized as follows. First, sea-ice dynamics equations which express the ice mass conservation and the linear momentum balance are formulated in Section 2. Then, in Section 3, constitutive relations describing the non-linearly viscous behaviour of ice are presented. This is followed by Section 4 in which the discrete SPH model is formulated for solving sea-ice dynamics problems. The result of numerical simulations carried out by using the SPH model are discussed in Section 5. Finally, some conclusions are drawn in the last Section 6.

2. Sea-ice Dynamics Equations

A typical sea-ice pack consists of a multitude of individual ice floes, varying in horizontal size and thickness, and of interspersed leads of water. Usually one can assume that the thickness of ice is small compared to the characteristic floe diameter, and that the latter is much smaller than the size of the whole pack. This allows us to treat an ice pack as a continuum on macroscopic scales of tens and hundreds of kilometres, with the local properties defined by ice thickness and ice area concentration. Equations governing the dynamics of sea ice and its constitutive behaviour can then be derived by applying standard methods of continuum mechanics. An example of such an approach is the theory proposed by Gray and Morland (1994), in which a horizontal two-dimensional formulation is developed by integrating through the ice thickness the mixture theory equations for the ice and lead water. The theoretical results obtained by Gray and Morland (1994) are used in the present analysis to construct a discrete SPH model for sea ice.

Sea ice pack behaviour is analysed in rectangular Cartesian coordinates, with origin O and the two coordinate axes, x_1 and x_2, placed on the horizontal plane defined by the mean sea level; for simplicity, the curvature of Earth's surface is neglected. Let t denote time, then the current position of an ice particle on the horizontal plane is defined by the position vector $\boldsymbol{x}(t)$, with components $x_i(t)$, $i = 1, 2$. The movement of the ice pack on the plane Ox_1x_2 is described by the horizontal velocity vector $\boldsymbol{v}(t)$, with components v_1 and v_2. It is assumed that the lead water moves horizontally with

the velocity of the local ice field. The pack layer has a local thickness defined by the function $h(\boldsymbol{x}, t)$. The latter is supposed to be a smooth function of $\boldsymbol{x}$, which is achieved by continuous extension of adjacent ice floe top and bottom surfaces in places where there is lead water, as depicted in Figure 1. In general, ice floes occupy only some fraction of the total surface of the ice–water system. This ice area fraction, denoted by the function $A(\boldsymbol{x}, t)$, which obviously has the property $0 \leq A \leq 1$, is referred to as the ice concentration.

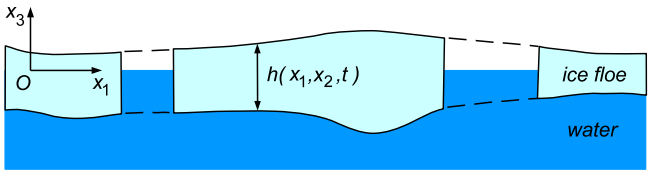

Fig. 1. Vertical cross-section through a sea-ice pack layer

2.1. Mass Conservation Equations

No thermodynamic effects in the ice–water–atmosphere system, such as ice melting and lead water freezing, or heat fluxes between the ice, water and air, are taken into account in this work. Therefore, the total mass of ice in the system considered remains constant. Under such assumptions, the mass conservation balance for the ice pack is expressed in terms of two equations, describing the evolution of the local ice thickness h and the local ice concentration A. These two equations are adopted in the following forms (Gray and Morland 1994, Morland and Staroszczyk 1998):

$$\frac{\mathrm{D}A}{\mathrm{D}t} + A\eta\left[1 - \alpha(A)H(-\eta)\right] = 0, \tag{1}$$

$$\frac{\mathrm{D}h}{\mathrm{D}t} + h\eta\alpha(A)H(-\eta) = 0. \tag{2}$$

In the above equations, $\mathrm{D}/\mathrm{D}t$ denotes the material (convected with the velocity field $\boldsymbol{v}$) time derivative. The quantity $\eta(\boldsymbol{x}, t)$ is the horizontal dilatation-rate, defined as the divergence of the horizontal velocity field of the ice pack:

$$\eta = \nabla \cdot \boldsymbol{v} = \frac{\partial v_1}{\partial x_1} + \frac{\partial v_2}{\partial x_2}, \tag{3}$$

with the properties

$$\eta \begin{cases} < 0 & \text{in converging flow,} \\ > 0 & \text{in diverging flow.} \end{cases} \tag{4}$$

In equation (3), ∇ denotes the nabla differential operator. The function $H(\cdot)$ entering equations (1) and (2) denotes the Heaviside unit step function, which is zero for the

negative values of its argument, and is unity for the positive values of the argument. Hence, by definition,

$$\eta \begin{cases} 1 \text{ for } \eta < 0, & \text{i.e. in converging flow,} \\ 0 \text{ for } \eta > 0, & \text{i.e. in diverging flow.} \end{cases} \tag{5}$$

The Heaviside function has been introduced to describe the very distinct sea-ice pack behaviour, depending on whether the ice is in diverging ($\eta > 0$) or converging ($\eta < 0$) flow. In the former case, of ($\eta > 0$), interactions between individual floes are rare or absent, so the interaction forces between adjacent floes are small or zero, while in the latter case, of ($\eta < 0$), interactions between floes are frequent or occurring at all times, and the corresponding interaction forces can attain large magnitudes.

We note that the presence of the $H(-\eta)$ terms in the mass conservation relations (1) and (2) considerably changes the formal structure of the equations involved as η changes its sign around the zero value. This feature is a source of considerable numerical difficulties when standard mesh-based methods, such as a finite-element method (Morland and Staroszczyk 1998), are employed to solve the sea-ice dynamics equations. It is expected that the application of the mesh-free SPH approach will help to alleviate these difficulties.

Important physical processes which take place in a converging flow of ice, during which individual ice floes collide, are the mechanisms of ice rafting and ridging (Babko et al 2002). In the first mechanism, colliding floes override one another, whereas the other mechanism is due to ice crushing and subsequent piling up of the ice rubble on the surfaces of colliding floes (which gives rise to so-called pressure ridges). Both mechanisms result in an increase in the local ice thickness and, in the absence of thermodynamic effects, can be regarded as irreversible phenomena. In order to incorporate these two processes into the formal description of the ice pack behaviour, a so-called ridging function, denoted here by $\alpha(A)$, is introduced (Hibler 1979). Gray and Morland (1994) postulated that a properly constructed ridging function should satisfy the conditions

$$\eta \geq 0: \quad \alpha = 0; \quad \eta < 0: \quad 0 \leq \alpha \leq 1; \quad \alpha \to 1 \quad \text{as} \quad A \to 1. \tag{6}$$

Accordingly, these authors proposed the following, piecewise linear form of the function $\alpha(A)$

$$\alpha(A) = \begin{cases} \dfrac{A - A_f}{1 - A_f} & \text{for} \quad 0 < A_f < A \leq 1, \\ 0, & \text{for} \quad 0 \leq A \leq A_f\,. \end{cases} \tag{7}$$

In the above relations, A_f denotes a critical ice concentration level, below which no ice ridging occurs (despite the converging flow regime), and above which $\alpha(A)$ increases continuously to the unit limit as A approaches unity. Two particular values of $A_f = 0.5$ and $A_f = 0.75$ were used in numerical simulations carried out by Gray and Morland (1994).

The form (7) is an improvement of the function originally proposed by Hibler (1979), which turned out to yield non-physical ice pack behaviour (ice concentration could exceed unity in sustained converging flow). In the present analysis, an alternative cubic relation in A is proposed, with the idea to smooth out the piecewise linear form (7), which is expected to improve the numerical performance of the SPH model. Hence, the following form is adopted:

$$\alpha(A) = \begin{cases} -2\left(\dfrac{A - A_f}{1 - A_f}\right)^3 + 3\left(\dfrac{A - A_f}{1 - A_f}\right)^2, & \text{for} \quad 0 < A_f < A \leq 1, \\ 0, & \text{for} \quad 0 \leq A \leq A_f\,. \end{cases} \tag{8}$$

2.2. Linear Momentum Equation

As already stated, it is assumed that the motion of a sea-ice pack is restricted to the horizontal plane Ox_1x_2; that is, the possible motion of ice in the vertical x_3-direction is neglected. The horizontal linear momentum equation governing the motion of the ice pack is derived (Gray and Morland 1994) by integrating full three-dimensional balances through the ice thickness to yield the expression

$$\rho h \frac{\mathrm{D}\boldsymbol{v}}{\mathrm{D}t} = \nabla \cdot \boldsymbol{N} + \boldsymbol{f}_a + \boldsymbol{f}_w + \boldsymbol{f}_c\,. \tag{9}$$

In the above equation, ρ denotes the intrinsic density of ice, with the value of $\rho = 917\ \mathrm{kg\,m^{-3}}$, $\boldsymbol{N}$, with components N_{11}, N_{12} and N_{22}, is the depth-integrated horizontal stress tensor (with physical dimension Pa · m), $\boldsymbol{f}_a$ and $\boldsymbol{f}_w$ denote external tractions exerted on the top and bottom surfaces of the ice cover by wind and water drag stress, respectively, and the term $\boldsymbol{f}_c$ represents the Coriolis force effect.

The two-dimensional stress $\boldsymbol{N}$ is a mean stress acting on a unit area of the aggregate consisting of ice floes and lead water. By analogy to the theory of two-phase media, it can be interpreted as the so-called partial stress, which is a product of the intrinsic stress, $\boldsymbol{\sigma}$, and the ice area fraction, A. Accordingly, $\boldsymbol{N}$ is expressed by the formula

$$\boldsymbol{N} = Ar(h)f(A)\,\boldsymbol{\sigma}. \tag{10}$$

The stress $\boldsymbol{\sigma}$ describes a mean value of stress per unit thickness of ice, and it acts when there is full contact between adjacent floes along their edges – such a situation occurs when the ice concentration A is equal to unity (which means that there is no lead water between the floes). The stress $\boldsymbol{\sigma}$ will be prescribed by a constitutive equation in terms of the rates of the horizontal deformation of the ice pack in Section 3.

The stress definition (10) includes two proportionality factors, $r(h)$ and $f(A)$. The first factor describes the effect of increasing ice thickness h on the depth-integrated stress $\boldsymbol{N}$, whereas the second factor, $f(A)$, is a measure of the floe–floe contact length, assumed to increase with the increasing ice concentration A. Two common forms of the factor $r(h)$ are a linear dependence on h and a quadratic function of h. Hence,

$$r(h) = h, \quad \text{or} \quad r(h) = \frac{h^2}{h^*}, \tag{11}$$

where h^* is a typical ice thickness scale. In this work only the simpler, linear form $r(h) = h$ will be used in numerical simulations. The dimensionless contact length function $f(A)$, necessarily with the properties $f(0) = 0$ and $f(1) = 1$, is adopted in the form proposed by Gray and Morland (1994):

$$f(A) = \frac{\exp[-K(1-A)] - \exp(-K)}{1 - \exp(-K)}, \quad K \gg 1. \tag{12}$$

It is a slight modification of an earlier formula proposed by Hibler (1979), according to whom the empirical parameter K should have a value of about 20.

The terms $\boldsymbol{f}_a$ and $\boldsymbol{f}_w$ appearing in the motion equation (9) represent tangential tractions acting on the top surface and the base of the ice cover. Similarly to the stress $\boldsymbol{N}$, these tractions also have the meaning of partial quantities, which are expressed in terms of the intrinsic tractions exerted by wind drag and water currents, denoted respectively by $\boldsymbol{\tau}_a$ and $\boldsymbol{\tau}_b$, and the ice area fraction A. Hence, they are defined by the relations

$$\boldsymbol{f}_a = A\boldsymbol{\tau}_a, \quad \boldsymbol{f}_w = A\boldsymbol{\tau}_w. \tag{13}$$

A number of relations expressing the intrinsic surface tractions in terms of the ice, wind and ocean current velocities are known in the literature, including forms which are linear or quadratic in the velocities. Linear relations were used, among others, by Hibler (1979), Flato and Hibler (1992), Gray and Morland (1994) and Morland and Staroszczyk (1998). In this work, quadratic formulae are adopted, expressed in the forms (Sanderson 1988)

$$\boldsymbol{\tau}_a = C_a\rho_{air}\boldsymbol{u}_a - \boldsymbol{v})|\boldsymbol{u}_a - \boldsymbol{v}|, \quad \boldsymbol{\tau}_w = C_w\rho_w(\boldsymbol{u}_w - \boldsymbol{v})|\boldsymbol{u}_w - \boldsymbol{v}|, \tag{14}$$

where ρ_{air} and ρ_w are, respectively, the air and water densities (with $\rho_w = 1028\ \mathrm{kg\,m^{-3}}$ for sea water and $\rho_{air} = 1.3\ \mathrm{kg\,m^{-3}}$ for air), and $\boldsymbol{u}_a$ and $\boldsymbol{u}_w$ are, respectively, the wind and ocean current velocity vectors. The parameters C_a and C_w in formulae (14) denote dimensionless wind stress and water drag coefficients. The particular values $C_a = 2 \times 10^{-3}$ and $C_w = 4 \times 10^{-3}$ will be used in numerical simulations presented in Section 5.

The last term on the right-hand side of equation (9), describing the Coriolis effect, is given by

$$\boldsymbol{f}_c = \rho h\boldsymbol{a}_c, \tag{15}$$

where $\boldsymbol{a}_c$ is the Coriolis acceleration vector defined by

$$\boldsymbol{a}_c = 2\boldsymbol{v} \times \boldsymbol{\Omega}. \tag{16}$$

In (16), $\boldsymbol{\Omega}$ is the vector of the angular velocity of Earth in its rotation about the north–south axis.

On account of the definitions (10), $(11)_1$, (13), (15) and (16), the momentum equation (9) takes the form

$$\rho h \frac{\mathrm{D}\boldsymbol{v}}{\mathrm{D}t} = Ahf(A)\nabla \cdot \boldsymbol{\sigma} + A\,(\boldsymbol{\tau}_a + \boldsymbol{\tau}_w) + 2\rho h\, \boldsymbol{v} \times \boldsymbol{\Omega}, \tag{17}$$

with the ice surface traction terms $\boldsymbol{\tau}_a$ and $\boldsymbol{\tau}_w$ given by relations (14).

3. Constitutive Description of Sea Ice

Various forms of constitutive laws describing the rheology of sea ice have been proposed so far, tested in numerical models and verified by field observations. These laws include, among others, non-linearly viscous, elastic-plastic, viscous-plastic, elastic-viscous-plastic and recently elastic-brittle constitutive models, all constructed with the purpose to describe as realistically as possible the complex behaviour of sea ice. In the present analysis we restrict ourselves to the non-linearly viscous fluid rheology. Once the proposed SPH model has been verified for this relatively simple form of the constitutive equation, more complex rheologies will be incorporated in the future into the SPH model.

Non-linearly viscous fluid models are usually derived from a general form of the Reiner-Rivlin constitutive equation (Chadwick 1999). In the context of sea ice applications, the first viscous fluid model was formulated by Smith (1983) and subsequently extended by Overland and Pease (1988) and a few other authors, including Gray and Morland (1994), Morland and Staroszczyk (1998) and Schulkes et al (1998). In general, the Reiner-Rivlin constitutive law expresses the Cauchy stress as a quadratic function of the strain-rate tensor and its three independent invariants. Here, a form linear in the strain-rate tensor is used, which is expressed in the form

$$\boldsymbol{\sigma} = \left[\phi_1(\eta,\gamma)\boldsymbol{I} + \phi_2(\eta,\gamma)\boldsymbol{D}\right] H(-\eta), \tag{18}$$

where $\boldsymbol{I}$ is the two-dimensional unit tensor, $\boldsymbol{D}$ is the two-dimensional strain-rate tensor, and ϕ_1 and ϕ_2 are the material response functions. The Heaviside function term $H(-\eta)$ is introduced in (18) with the purpose of setting the stress to zero in a diverging flow of the sea-ice pack. The strain-rate tensor $\boldsymbol{D}$ has components

$$D_{ij} = \frac{1}{2}\left(\frac{\partial v_i}{\partial x_j} + \frac{\partial v_j}{\partial x_i}\right) \quad (i,j = 1,2), \tag{19}$$

and η and γ, which are strain-rate invariants of $\boldsymbol{D}$, are given by

$$\eta = \mathrm{tr}\boldsymbol{D}, \quad \gamma^2 = \frac{1}{2}\mathrm{tr}\boldsymbol{D}^2. \tag{20}$$

In the above definition, tr(·) denotes the trace of a tensor, and $\hat{\boldsymbol{D}}$ is the deviatoric strain-rate tensor given by

$$\hat{\boldsymbol{D}} = \boldsymbol{D} - \frac{1}{2}\eta \boldsymbol{I}. \tag{21}$$

Obviously, the above definition for η is equivalent to that given earlier by relation (3). In strain-rate components, the two invariants, the dilatation-rate η and the shear-rate invariant γ, are expressed by

$$\eta = D_{11} + D_{22}, \quad \gamma^2 = D_{12}^2 + \frac{1}{4}(D_{11} - D_{22})^2. \tag{22}$$

Similarly to (21), the stress tensor $\boldsymbol{\sigma}$ is also decomposed into its axial and deviatoric parts as follows:

$$\hat{\boldsymbol{\sigma}} = \boldsymbol{\sigma} + p\boldsymbol{I}, \quad p = -\frac{1}{2}\mathrm{tr}\boldsymbol{\sigma}, \tag{23}$$

where p is the mean pressure in ice.

The two constitutive functions ϕ_1 and ϕ_2 appearing in the general law (18) describe the response of the medium to the applied strain-rates. These functions can be expressed (Morland and Staroszczyk 1998, Staroszczyk 2005) in terms of conventionally used bulk and shear viscosities, ζ and μ respectively, defined by

$$p = -\zeta\eta, \quad \hat{\boldsymbol{\sigma}} = 2\mu\hat{\boldsymbol{D}}, \tag{24}$$

where $\hat{\boldsymbol{\sigma}}$ is the deviatoric stress tensor. On account of these definitions, the response functions ϕ_1 and ϕ_2 are given by

$$\phi_1 = (\zeta - \mu)\eta, \quad \phi_2 = 2\mu, \tag{25}$$

and the viscous flow law (18) becomes

$$\boldsymbol{\sigma} = \left[(\zeta - \mu)\eta\boldsymbol{I} + 2\mu\boldsymbol{D}\right] H(-\eta). \tag{26}$$

A reduced version of the above law, obtained by setting $\zeta = \mu$, implying $\phi_1 = 0$, was used by Schulkes et al (1998). Note that (26) is, in general, a non-linear law, since the viscosities ζ and μ are the functions of the strain-rate invariants η and γ. An example of the non-linearly viscous rheology is the constitutive model proposed by Overland and Pease (1988), in which the function ϕ_1 is assumed to depend on the state variables h and A, and the function ϕ_2 (describing the deviatoric stress) depends on the shear-rate invariant γ. With the specific forms of ϕ_1 and ϕ_2 considered by Schulkes et al (1998)

$$\phi_1 = h, \quad \phi_2 = \frac{D_0}{\gamma_0 + \gamma}\,\phi_1, \tag{27}$$

where D_0 and γ_0 are empirical constants, the viscous flow law becomes

$$\boldsymbol{\sigma} = h\left(\boldsymbol{I} + \frac{D_0}{\gamma_0 + \gamma}\,\boldsymbol{D}\right) H(-\eta). \tag{28}$$

In view of definition (10), the depth-integrated stress $\boldsymbol{N}$ determined by the law (28) depends on the ice thickness h in a quadratic manner, unlike the law (26), in which this dependence is linear in h.

4. Smoothed Particle Hydrodynamics Formulation

In the SPH approach, a continuum is represented by a collection of discrete particles, each of which carries, in a Lagrangian sense, information on local physical properties (mass, density, velocity, temperature, etc.) of the system under consideration. Since no numerical grids or pre-defined connections between particles are required in this method, it has a great flexibility of dealing with large medium deformations, material fragmentation, propagation of discontinuity fronts, etc. Approximation of field variables on the basis of their values given at discrete particles is performed by using special interpolating functions, usually referred to as smoothing kernels. Typically, a smoothing kernel has non-zero values only in a small domain, called the kernel support. Most often, the latter has the shape of a circle or sphere centred at a given material particle or spatial point (see Fig. 2). Details on the SPH methodology can be found in the literature, for instance in many papers by Monaghan (1992, 2005, 2012), the co-inventor of this method, or in the book by Li and Liu (2004).

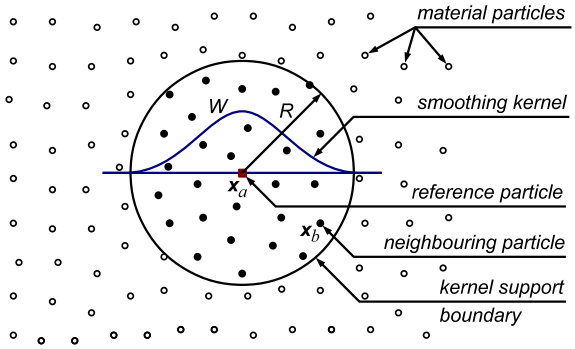

Fig. 2. The method of approximation of field variables in the SPH. The approximation at a reference particle $\boldsymbol{x}_a$ (solid square) involves material particles $\boldsymbol{x}_b$ (solid circles) situated within a circular support domain of radius R centred at $\boldsymbol{x}_a$. Particles outside the support domain (empty circles) do not contribute to the approximation of field functions at the reference particle $\boldsymbol{x}_a$. W denotes a smoothing kernel function centred at $\boldsymbol{x}_a$.

The values of field variables at any point $\boldsymbol{x}$ of a continuum are calculated by summations over all particles contained within the kernel support. Similarly, the spatial derivatives of field functions are evaluated by summation formulae involving spatial derivatives of the smoothing kernel functions (which, along with their derivatives, are defined by analytical expressions). Accordingly, the value of a function f at position $\boldsymbol{x}_a$ is evaluated by means of a kernel function, W, centred at this particle, by the formula

$$f_a = f(\boldsymbol{x}_a) = \sum_{b=1}^{N} V_b\, f_b\, W(r_{ab})\,. \tag{29}$$

In (29), a and b denote particle labels, $f_a = f(\boldsymbol{x}_a)$ is a discrete value of f at particle a, N denotes the number of discrete particles currently located within the kernel support domain of particle a, V_b is the volume of particle b, and $r_{ab} = |\boldsymbol{x}_{ab}| = |\boldsymbol{x}_a - \boldsymbol{x}_b|$ is the distance between particles a and b.

In order to express the differential equations of the problem in their discrete SPH forms, one needs approximations of differential operators. Inspection of equations (1), (2) and (17), together with the definition (3) of the dilatation-rate η, shows that only the approximations of the divergence operators for vector and tensor fields are needed in this analysis. These approximations are adopted in the forms recommended by Monaghan (1992) and Gray et al (2001):

$$(\nabla \cdot \boldsymbol{f})_a = -\frac{1}{\rho_a} \sum_{b=1}^{N} m_b\, \boldsymbol{f}_{ab} \cdot \nabla_a W_{ab} \tag{30}$$

and

$$(\nabla \cdot \boldsymbol{A})_a = \rho_a \sum_{b=1}^{N} m_b \left(\frac{\boldsymbol{A}_a}{\rho_a^2} + \frac{\boldsymbol{A}_b}{\rho_b^2} \right) \cdot \nabla_a W_{ab}\,. \tag{31}$$

In the above two expressions, $\boldsymbol{f}$ and $\boldsymbol{A}$ denote, respectively, a vector and a two-dimensional tensor field, ρ_a is the density of particle a, m_b is the mass of particle b, and $\boldsymbol{f}_{ab} = \boldsymbol{f}_a - \boldsymbol{f}_b$. $\nabla_a W_{ab}$ denotes the gradient of the kernel function W centred at particle a and calculated at particle b. This gradient is defined by

$$\nabla_a W_{ab} = \frac{\boldsymbol{x}_{ab}}{r_{ab}} \frac{\partial W(r_{ab})}{\partial r_{ab}}\,. \tag{32}$$

On application of the divergence operator approximations (30) and (31), the mass conservation balances (1) and (2) and the momentum equation (17) become

$$\frac{\mathrm{d}A_a}{\mathrm{d}t} = -A_a \eta_a \left[1 - \alpha(A_a) H(-\eta_a)\right], \tag{33}$$

$$\frac{\mathrm{d}h_a}{\mathrm{d}t} = -h_a \eta_a \alpha(A_a) H(-\eta_a), \tag{34}$$

$$\frac{\mathrm{d}\boldsymbol{v}_a}{\mathrm{d}t} = \frac{\rho_a}{\rho} A_a\, f(A_a) \sum_{b=1}^{N} m_b \left(\frac{\boldsymbol{\sigma}_a}{\rho_a^2} + \frac{\boldsymbol{\sigma}_b}{\rho_b^2} \right) \cdot \nabla_a W_{ab} + \frac{A_a}{\rho h_a} (\tau_a + \tau_w)_a\,. \tag{35}$$

Recall that the stress $\boldsymbol{\sigma}$ is defined by the constitutive laws (26) or (28). In equation (35), the Coriolis acceleration term has been ignored, as the Coriolis effect can be

neglected on the moderate length scales considered here. The ice dilatation-rate η, when approximated at particle a, is given by

$$\eta_a = (\nabla \cdot \boldsymbol{v})_a = -\frac{1}{\rho_a} \sum_{b=1}^{N} m_b \boldsymbol{v}_{ab} \cdot \nabla_a W_{ab} \,, \tag{36}$$

where $\boldsymbol{v}_{ab} = \boldsymbol{v}_a - \boldsymbol{v}_b$. In addition to relations (33)–(35), in order to trace the motion of ice on the sea surface, a trajectory equation has also to be solved for each discrete particle:

$$\frac{\mathrm{d}\boldsymbol{x}_a}{\mathrm{d}t} = \boldsymbol{v}_a \,. \tag{37}$$

The above system of equations (33)–(35) and (37) for particle a is equivalent to six scalar relations for unknown field functions: A, h, two components of the velocity vector $\boldsymbol{v}$, and two components of the position vector $\boldsymbol{x}$. This system of six equations, in order to integrate them in the time domain, is solved separately for each discrete particle by a predictor-corrector method (Staroszczyk 2010, 2011).

It should be pointed out that in the above formulae there is an important qualitative difference between the ice intrinsic density ρ, which is treated as constant, and the densities ρ_a and ρ_b of discrete particles, which vary in time. The latter densities connect discrete particle masses (which are constant when there are no thermodynamic phenomena involved) with discrete particle volumes (which change in time as ice pack deforms) through the relation

$$m_a = \rho_a V_a \,, \tag{38}$$

where the particle density ρ_a is related, in turn, to the local ice concentration A_a and the local ice thickness h_a by the formula

$$\rho_a = \rho A_a h_a \,. \tag{39}$$

Hence, the particle density ρ_a expresses the mass of ice per unit surface of the sea, so that it has the meaning of the partial density, and its physical unit is kg m^{-2}.

5. Numerical Simulations

The proposed SPH model has been applied to simulate the dynamic behaviour of an ice pack under the action of wind and water drag stresses. Hence, an initial boundary value problem was solved, defined by the ice thickness and ice concentration evolution equations (1) and (2) and the momentum equation (17). The initial conditions at the start of ice flow at time $t_0 = 0$ were prescribed by

$$A(\boldsymbol{x}, t_0) = A_0(\boldsymbol{x}), \quad h(\boldsymbol{x}, t_0) = h_0(\boldsymbol{x}), \quad \boldsymbol{v}(\boldsymbol{x}, t_0) = \boldsymbol{0}. \tag{40}$$

The boundary conditions at the ice pack–open sea interfaces were assumed to be stress-free, and the conditions at the ice–solid boundaries were taken as either bonded

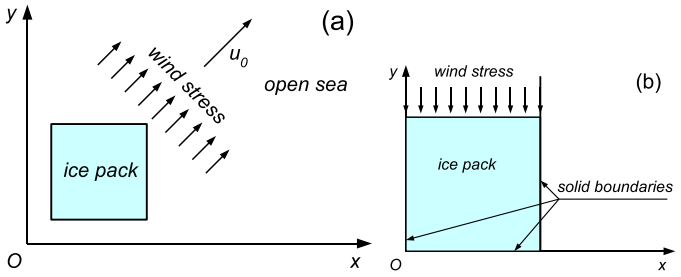

Fig. 3. Simple ice pack flow configurations

(zero tangential and normal velocities), or slip-free (zero tangential traction and zero normal velocity).

Before starting the proper ice pack flow simulations, the model was tested on a range of simple problems, sketched in Fig. 3. The problem shown in Fig. 3a represents a free drift of a quadratic in plane shape ice pack of uniform thickness and ice concentration, driven into the open sea by wind-induced stresses uniform in space and time. The simulations where run for a period of a few days, with the wind velocity magnitude $u_0 = |\boldsymbol{u}_w| = 20$ m s^{-1}. The results for different combinations of h_0 and A_0, obtained by integrating the ice dynamics equations with a time-step length $\Delta t = 0.01$ hr (hour), showed that the ice pack preserved its initial shape and initial free-stress state over the whole period of simulations, and its free-drift velocity $|\boldsymbol{v}|$ matched accurately the ice velocity magnitude $|\boldsymbol{v}|$ determined by solving the two equations (14) for the equilibrium condition $\boldsymbol{\tau}_a + \boldsymbol{\tau}_w = \boldsymbol{0}$, with $\boldsymbol{u}_w = \boldsymbol{0}$.

The simple flow problem depicted in Fig. 3b was solved by adopting either free-slip or no-slip conditions along the solid boundaries. The ice pack had the initial horizontal dimensions 20 km × 20 km and was driven by wind of the velocity 10 m s^{-1}, blowing in the direction normal to the coastline at $y = 0$. The initial ice thickness and concentration were $h_0 = 0.2$ m and $A_0 = 0.6$ throughout the pack, the adopted critical ice concentration parameter was $A_f = 0.5$, and the ice viscosity parameters in the constitutive law (26) were $\zeta = 2 \times 10^9$ Pa· s and $\mu = 1 \times 10^9$ Pa· s. The results presented below were obtained for an initial inter-particle spacing equal to $d = 1$ km, so that the computational grid consisted of 400 discrete particles. The smoothing kernel function W was adopted in the form of a quintic spline function proposed by Morris (1996), with the kernel support domain radius $R = 4d$. In order to trace more accurately the current position of the moving ice pack–open sea boundaries, the standard smoothing kernels and their gradients were modified by following an approach proposed by Belytschko et al (1998) (this technique is known as the corrected smoothed particle hydrodynamics, C-SPH).

The case of free-slip conditions along solid boundaries corresponds to a one-dimensional configuration of ice flow along the negative direction of the y-axis. The results showing the ice concentration and thickness fields predicted by the SPH model

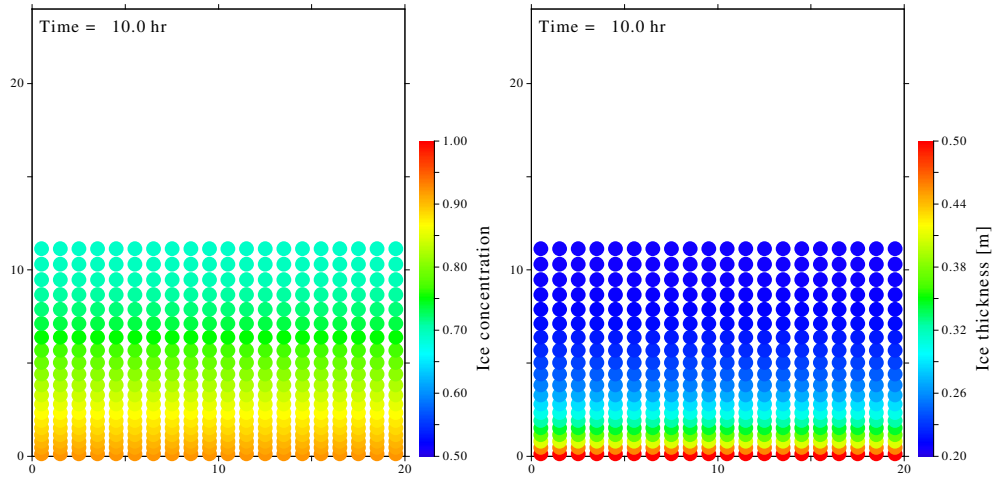

Fig. 4. Distributions of ice concentration and thickness after 10 hours of flow in the configuration shown in Fig. 3b, with free-slip conditions along solid boundaries (wind speed 10 m s^{-1}, $A_0 = 0.6$, $h_0 = 0.2$ m)

after a time of 10 hr (hours) are illustrated in Fig. 4. The plots demonstrate a significant increase in both ice thickness and ice concentration near the coastline $y = 0$, and show that the SPH model, even with a relatively coarse grid of particles, can successfully deal with large horizontal deformations of the ice pack along its flow direction.

Corresponding to Fig. 4 are the plots presented in Fig. 5, showing the profiles of ice concentration, thickness and horizontal velocity along the y-axis at different times. The right-hand ends of the curves show the y-positions of the free edge of the ice pack at given times.

A fully two-dimensional ice flow configuration arises when no-slip conditions are assumed along the solid boundaries shown in Fig. 3b. The evolution of the ice concentration and ice thickness fields in this flow configuration is illustrated in Fig. 6. All the parameters defining the flow problem had the same values as in the previous case of free-slip boundary conditions. One can see that again, despite the relatively coarse grid of discrete particles, the proposed SPH model yields smooth solutions.

The corresponding profiles of the ice concentration, thickness and horizontal velocity along the axis of the pack symmetry are presented in Fig. 7.

A much more challenging, in terms of numerics, is the ice pack flow configuration depicted in Fig. 8. In this flow problem, an ice pack initially occupies a rectangular domain $L_1 \times L_2$, with three sides (Γ_1, Γ_2 and Γ_3) of the ice pack domain being constrained by solid boundaries, and the fourth side (Γ_4) being an open water boundary. It is assumed that the ice pack is driven by a vortex geostrophic wind field, with the vortex centre, marked by the cross in the figure, located at the open sea at some distance from the initial line of the ice pack edge Γ_4. The vortex wind velocity field $\boldsymbol{u}_a$ is described by the formula

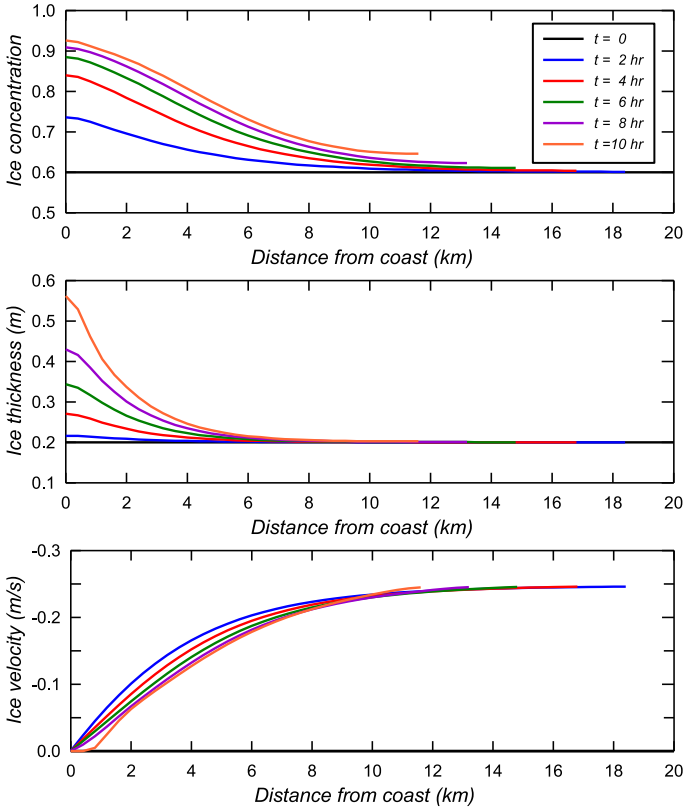

Fig. 5. Evolution of the profiles of ice concentration, ice thickness and ice horizontal velocity along the y-axis for the flow domain shown in Fig. 3b, with free-slip conditions along solid boundaries (wind speed 10 m s^{-1}). The same labelling applies to all three plots

$$\boldsymbol{u}_a(\boldsymbol{R}) = u_0 \cdot \min\left(\frac{|\boldsymbol{R}|}{R_0}, \frac{R_0}{|\boldsymbol{R}|}\right) \boldsymbol{k} \times \frac{\boldsymbol{R}}{|\boldsymbol{R}|}, \tag{41}$$

where $\boldsymbol{R}$ is the vector radius from the vortex centre and $|\boldsymbol{R}|$ is its magnitude, R_0 is the distance from the vortex centre where the wind velocity $\boldsymbol{u}_a$ attains its maximum magnitude equal to u_0, and $\boldsymbol{k}$ denotes an upward vertical unit vector (normal to the plane Oxy). In view of (41), the wind velocity increases linearly from zero to u_0 at R_0 and then gradually decreases to zero at $|\boldsymbol{R}| \to \infty$. In order to calculate the ice surface and basal tractions, τ_a and τ_w respectively, see formulae (14), the wind and ice velocity vectors, $\boldsymbol{u}_a$ and $\boldsymbol{v}$, must be rotated on the horizontal plane by applying the relations

$$\bar{\boldsymbol{u}}_a = \boldsymbol{u}_a \cos\theta_a + \boldsymbol{k} \times \boldsymbol{u}_a \sin\theta_a, \tag{42}$$

$$\bar{\boldsymbol{v}} = \boldsymbol{v} \cos\theta_w + \boldsymbol{k} \times \boldsymbol{v} \sin\theta_w. \tag{43}$$

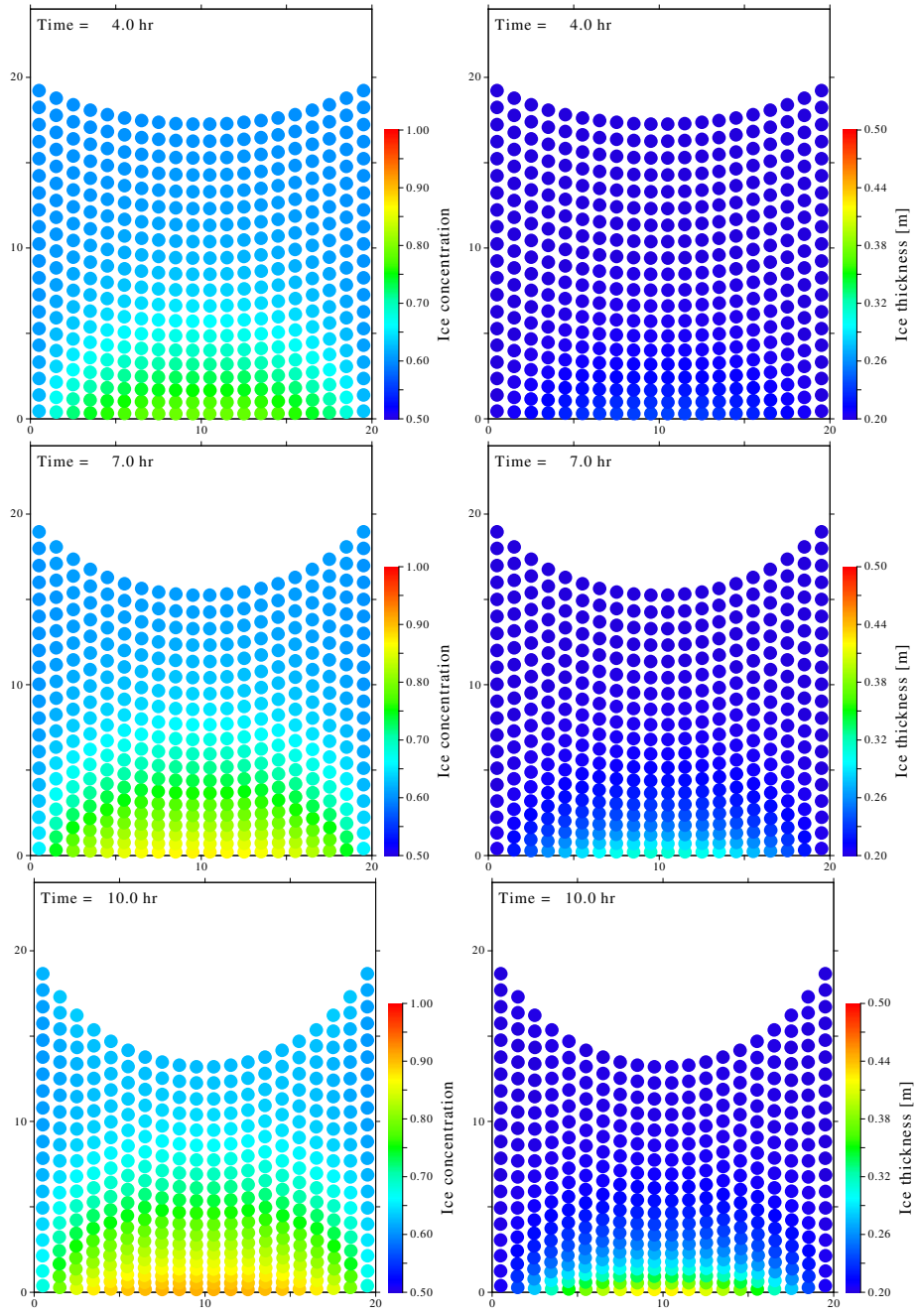

Fig. 6. Evolution of ice concentration and thickness in the flow configuration shown in Fig. 3b, with no-slip conditions along solid boundaries (wind speed 10 m s^{-1}, $A_0 = 0.6$, $h_0 = 0.2$ m)

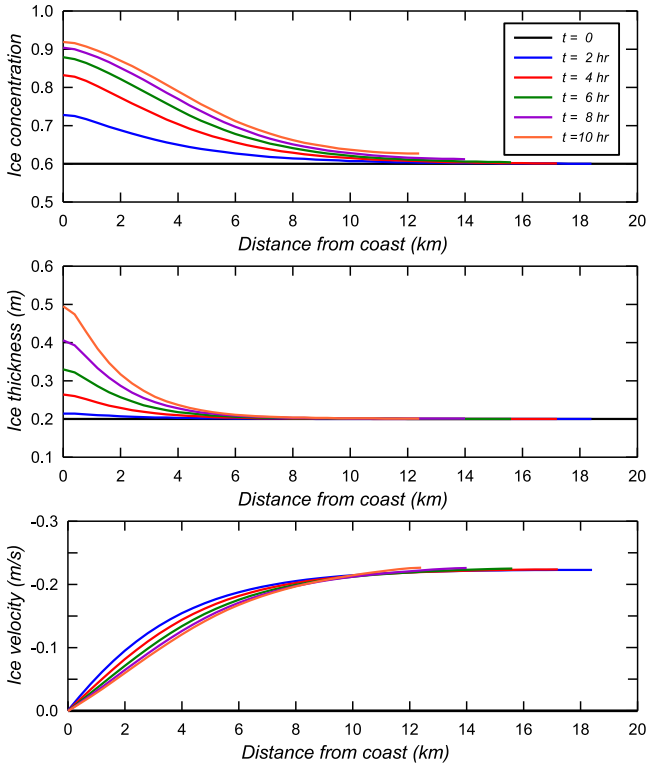

Fig. 7. Evolution of the profiles of ice concentration, ice thickness and ice velocity along the symmetry axis of the flow domain shown in Fig. 3b, with no-slip conditions along solid boundaries (wind speed 10 m s^{-1}). The same labelling applies to all three plots

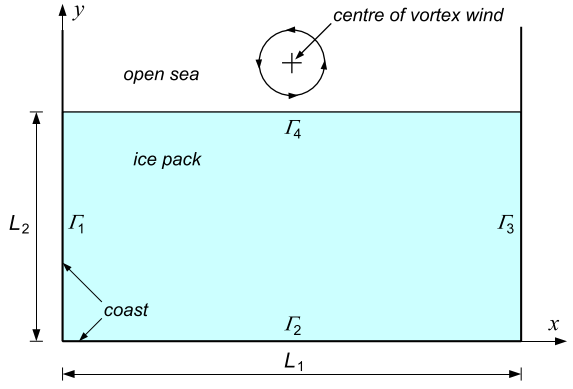

Fig. 8. Rectangular ice pack with three solid boundaries (Γ_1, Γ_2 and Γ_3) and one open water boundary (Γ_4), driven by a vortex wind field with the vortex centre, indicated by the cross, located at the open sea

In these expressions, θ_a and θ_w are the wind and water turning angles related to the planetary boundary layer; both these angles are assumed to be equal to 25° (Flato 1993).

The numerical simulations were run for ice pack dimensions $L_1 = 400$ km and $L_2 = 200$ km, with the wind vortex centre situated 50 km from the initial line of the ice pack edge Γ_4. The maximum wind speed, at a distance of $R_0 = 40$ km from the vortex centre, was assumed to be $u_0 = 20\ \mathrm{m\,s^{-1}}$. The initial ice thickness was $h_0 = 1$ m and the initial ice concentration was $A_0 = 0.6$, with the critical concentration level $A_f = 0.5$. The ice viscosity magnitudes were again $\zeta = 2 \times 10^9$ Pa · s and $\mu = 1 \times 10^9$ Pa · s. The computational grid in the initial configuration consisted of $80 \times 40 = 3200$ discrete particles uniformly distributed along the directions of both coordinate axes, with the initial inter-particle spacings $d = 5$ km. Free-slip conditions were adopted along the coastlines Γ_1, Γ_2 and Γ_3.

The results of the simulations have shown that the proposed SPH model, despite large deformations of the ice pack flow domain, yields smooth solutions and is capable of tracking large displacements of the ice pack–open sea boundary. This is illustrated by the plots in Fig. 9, showing the discrete particle configurations at the start of flow and after eight days of the pack deformation. The colours of the particles have no physical meaning and are used only for illustrating the pattern of the deformation field. One can see that the largest displacements of the material particles of ice, after eight days, exceed 100 km (the 'tongue' of the ice pack), with smaller displacements, of about 70 km occurring along the solid boundaries Γ_1 and Γ_3.

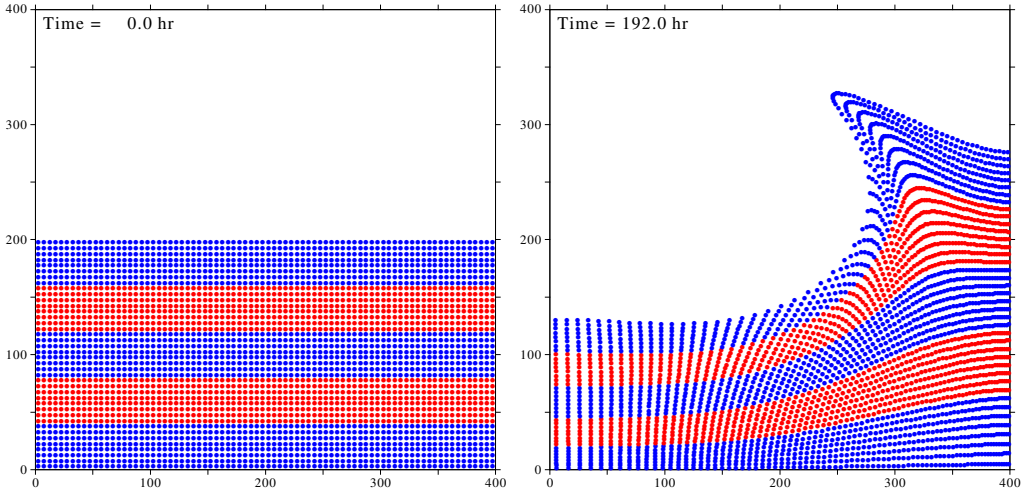

Fig. 9. Evolution of the initially rectangular ice pack shown in Fig. 8, with free-slip conditions along coastlines. Discrete particle distributions at the start of flow and after eight days

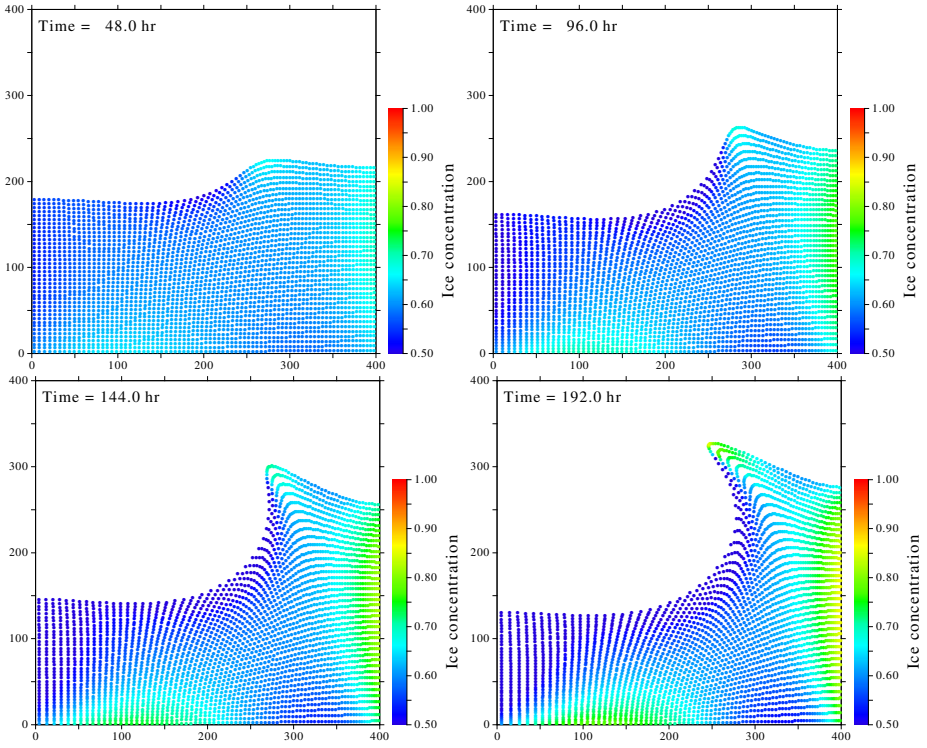

Fig. 10. Evolution of the initially rectangular ice pack shown in Fig. 8, with free-slip conditions along coastlines. Ice concentration distributions after two, four, six and eight days ($A_0 = 0.6$)

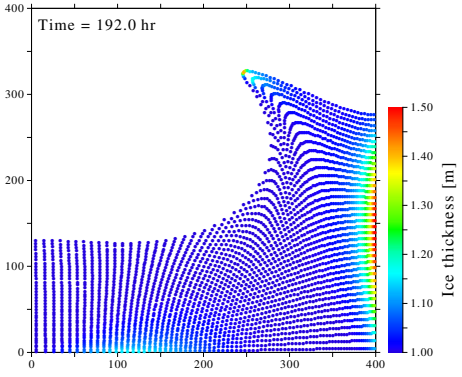

Fig. 11. Flow of the initially rectangular ice pack shown in Fig. 8, with free-slip conditions along coastlines. Ice thickness distribution after eight days ($h_0 = 1.0$ m)

The following Fig. 10 shows the evolution of the ice concentration $A(x, y, t)$, and displays ice concentration fields after two, four, six and eight days ($t = 192$ hr) of the simulations. It is seen that the largest increase in the ice area fraction A, from its

initial value$A_0 = 0.6$, occurs along the coastline Γ_3, towards which the ice is pushed by the vortex wind field. A relatively smaller increase in A is observed along the boundary Γ_2, with the maximum values around $x \approx 150$ km. Significant changes in the ice concentration also take place at the tip of the ice pack tongue. In contrast to the ice area fraction field, changes in the ice thickness $h(x, y, t)$ are much less pronounced and essentially confined to the immediate vicinity of the boundary Γ_3, as can be seen in Fig. 11, showing the ice thickness distribution after eight days of the pack flow. Related to the results presented in Fig. 10 and 11 are the plots in Fig. 12, illustrating changes in time of the ice concentration and ice thickness along the coastline Γ_3 at $x = 400$ km; that is, along the y-axis direction. As previously in Fig. 5 and 7, the right-hand ends of the curves show the changing y-position of the ice pack–open sea boundary along the coastline Γ_3.

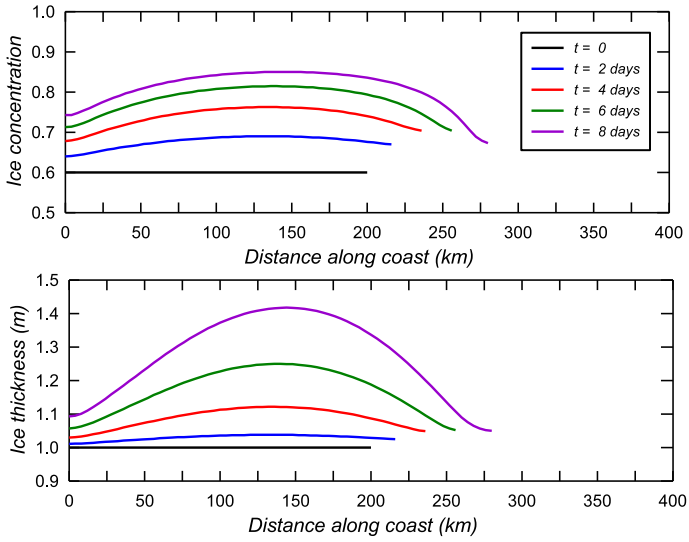

Fig. 12. Evolution of the profiles of ice concentration and ice thickness along the coastline Γ_3 (at $x = 400$ km) in the ice pack flow problem defined in Fig. 8. The same labelling applies to both plots

6. Conclusions

In the paper, a smoothed particle hydrodynamics model was developed for the purpose of modelling sea ice dynamics phenomena occurring on geophysical scales. The SPH model was used to simulate the evolution of a large sea-ice pack driven by wind and water drag stresses, with the primary interest in determining the variations in time and space of the ice concentration and ice thickness fields. It was assumed in the paper that the sea-ice rheology can be approximated by a non-linearly viscous fluid model with two viscosity parameters.

The proposed SPH model was first tested by simulating flows with simple initial configurations of an ice pack, and then was applied to simulate the behaviour of a large pack driven by a vortex wind. The results of these simulations demonstrated that by representing the sea-ice cover by an assembly of unconnected Lagrangian material particles it was possible to successfully treat large displacements and deformations observed in Arctic and Antarctic ice packs, and to track the changing position of an unconstrained ice pack edge. Although the predictions of the model seem to realistically reflect the main features of sea-ice pack flows, one has to note that the results of calculations have not been validated yet against data from in situ observations. Such a validation is intended after the proposed SPH model has been extended by incorporating also other rheological descriptions, accounting for the viscoplastic and brittle behaviour of sea ice.

References

Babko O., Rothrock D. A. and Maykut G. A. (2002) Role of rafting in the mechanical redistribution of sea ice thickness, *J. Geophys. Res.*, **107** (C8), 3113, DOI: 10.1029/1999JC000190.

Belytschko T., Krongauz Y., Dolbow J. and Gerlach C. (1998) On the completeness of meshfree particle methods, *Int. J. Numer. Meth. Eng.*, **43** (5), 785–819, DOI: 10.1002/(SICI)1097-0207(19981115)43:5.

Chadwick P. (1999) *Continuum Mechanics: Concise Theory and Problems*, Dover, Mineola, New York, 2nd edn.

Flato G. M. (1993) A particle-in-cell sea-ice model, *Atmos.-Ocean*, **31** (3), 339–358.

Flato G. M. and Hibler W. D. (1992) Modeling pack ice as a cavitating fluid, *J. Phys. Oceanogr.*, **22** (6), 626–651.

Gray J. M. N. T. and Morland L. W. (1994) A two-dimensional model for the dynamics of sea ice, *Phil. Trans. R. Soc. Lond.*, A 347 (1682), 219–290, DOI: 10.1098/rsta.1994.0045.

Gray J. P., Monaghan J. J. and Swift R. P. (2001) SPH elastic dynamics, *Comput. Meth. Appl. Mech. Eng.*, **190** (49-50), 6641–6662, DOI: 10.1016/S0045-7825(01)00254-7.

Gutfraind R. and Savage S. B. (1997) Marginal ice zone rheology: Comparison of results from continuum-plastic models and discrete-particle simulations, *J. Geophys. Res.*, **102** (C6), 12,647–12,661, DOI: 10.1029/97JC00124.

Gutfraind R. and Savage S. B. (1998) Flow of fractured ice through wedge-shaped channels: smoothed particle hydrodynamics and discrete-element simulations, *Mech. Mater.*, **29** (1), 1–17.

Hibler W. D. (1977) A viscous sea ice law as a stochastic average of plasticity, *J. Geophys. Res.*, **82** (27), 3932–3938.

Hibler W. D. (1979) A dynamic thermodynamic sea ice model, *J. Phys. Oceanogr.*, **9** (4), 815–846.

Li S. and Liu W. K. (2004) *Meshfree Particle Methods*, Springer, Berlin.

Monaghan J. J. (1992) Smoothed particle hydrodynamics, *Annu. Rev. Astron. Astrophys.*, **30**, 543–574, DOI: 10.1146/annurev.aa.30.090192.002551.

Monaghan J. J. (2005) Smoothed particle hydrodynamics, *Rep. Prog. Phys.*, **68** (8), 1703–1759, DOI: 10.1088/0034-4885/68/8/R01.

Monaghan J. J. (2012) Smoothed particle hydrodynamics and its diverse applications, *Annu. Rev. Fluid Mech.*, **44**, 323–346, DOI: 10.1146/annurev-fluid-120710-101220.

Morland L. W. and Staroszczyk R. (1998) A material coordinate treatment of the sea-ice dynamics equations, *Proc. R. Soc. Lond.*, A **454** (1979), 2819–2857, DOI: 10.1098/rspa.1998.0283.

Morris J. P. (1996) *Analysis of Smoothed Particle Hydrodynamics with Applications*, Ph.D. thesis, Monash University, Melbourne, Australia.

Overland J. E. and Pease C. H. (1988) Modeling ice dynamics of coastal seas, *J. Geophys. Res.*, **93** (C12), 15,619–15,637, DOI: 10.1029/JC093iC12p15619.

Sanderson T. J. O. (1988) *Ice Mechanics. Risks to Offshore Structures*, Graham and Trotman, London.

Schulkes R. M. S. M., Morland L. W. and Staroszczyk R. (1998) A finite-element treatment of sea ice dynamics for different ice rheologies, *Int. J. Numer. Anal. Meth. Geomech.*, **22** (3), 153–174.

Shen H. T., Su J. and Liu L. (2000) SPH simulation of river ice dynamics, *J. Comput. Phys.*, **165** (2), 752–770, DOI: 0.1006/jcph.2000.6639.

Smith R. B. (1983) A note on the constitutive law for sea ice, *J. Glaciol.*, **29** (101), 191–195.

Staroszczyk R. (2005) Loads exerted by floating ice on a cylindrical structure, *Arch. Hydro-Eng. Environ. Mech.*, **52** (1), 39–58.

Staroszczyk R. (2010) Simulation of dam-break flow by a corrected smoothed particle hydrodynamics method, *Arch. Hydro-Eng. Environ. Mech.*, **57** (1), 61–79.

Staroszczyk R. (2011) Simulation of solitary wave mechanics by a corrected smoothed particle hydrodynamics method, *Arch. Hydro-Eng. Environ. Mech.*, **58** (1-4), 23–45, DOI: 10.2478/v10203-011-0002-9.